PCCP

Theoretical investigation of defective MXenes as potential electrocatalysts for CO reduction toward C2 products

Journal:	*Physical Chemistry Chemical Physics*
Manuscript ID	CP-ART-03-2021-001291.R1
Article Type:	Paper
Date Submitted by the Author:	29-Apr-2021
Complete List of Authors:	Qian, Xu; Ningbo Institute of Materials Technology and Engineering Chinese Academy of Sciences Li, Lei ; University of Electronic Science and Technology of China, School of materials and energy; University of Science and Technology of China, Hefei National Laboratory for Physical Sciences at Microscale Li, Yanle; Ningbo Institute of Materials Technology and Engineering Chinese Academy of Sciences Liu, Zeyu; Jiangsu University of Science and Technology, College of Biotechnology and Sericultural Research Institute Tian, Ziqi; Institute of Materials Technology and Engineering, Chinese Academy of Sciences, Zhan, Cheng; Lawrence Livermore National Laboratory, Material Science Division Chen, Liang; Institute of Materials Technology and Engineering, Chinese Academy of Sciences,

Theoretical investigation of defective MXenes as potential electrocatalysts for CO reduction toward C_2 products

Xu Qian,[1,2,3] Lei Li,[1,2] Yanle Li,[1,2] Zeyu Liu,[4] Ziqi Tian,*[1,2] Cheng Zhan,*[5] Liang Chen*[1,2]

[1]Ningbo Institute of Materials Technology and Engineering, Chinese Academy of Sciences, Ningbo 315201, Zhejiang, China.

[2]University of Chinese Academy of Sciences, 100049, Beijing, China.

[3]Nano Science and Technology Institute, University of Science and Technology of China, Suzhou, 215123, China

[4]School of Environmental and Chemical Engineering, Jiangsu University of Science and Technology, Zhenjiang 212018, People's Republic of China

[5]Department of Chemistry, University of California, Riverside, California 92521, United States

Email: tianziqi@nimte.ac.cn; zhan1@llnl.gov; chenliang@nimte.ac.cn

Abstract

Electrochemical CO_2/CO conversion to valuable chemical products is an attractive strategy for storage of clean energy and control of greenhouse gas emission. Currently, CO_2 reduction to CO is relatively mature, whereas the deep reduction and further conversion of CO into multi-carbon products, such as ethylene (C_2H_4) and ethanol (C_2H_5OH), are highly challenging. Based on the density functional theory (DFT) calculations, we explored the possibility of CO reduction reaction (CORR) to C_2 products on defective MXenes in which the defect is created by removing two

neighboring oxygen atoms on surface. Our results revealed that the dual-oxygen vacancy in defective $Mo_2TiC_2O_2$ (labeled as $Mo_2TiC_2O_2$-$2O_V$) can offer a unique environment that confines and enriches the active *COH species, significantly promoting the reduction process as well as C-C bond coupling. The thermodynamic barrier of the potential-determining step (PDS) for $Mo_2TiC_2O_2$-$2O_V$ is 0.32 eV with promising selectivity of C_2 products over competing hydrogen evolution reaction (HER). This work provides feasible strategy of designing the MXene-based electrocatalysts for highly efficient CO_2/CO reduction to C_2 products.

Keywords: Density functional theory; Defective MXene; Electrocatalyst; CO reduction reaction; Dual-oxygen vacancy

1. Introduction

The extensive consumption of fossil fuels produces huge amount of carbon oxides, including CO_2 and CO, leading to serious environmental issues.[1-3] The widespread application of clean energy is urgently required for sustainable development.[4, 5] Electrocatalytic conversion of carbon oxides is of great importance in both carbon recycling and the storage of intermittent renewable electricity.[6-8] The two-electron reduction of CO_2 to CO has been well understood, while the mechanistic understanding of CO reduction to multi-carbon products, such as ethylene[9-11] and liquid oxygenates[12, 13], is still limited and has more space to explore. In addition, CO can be obtained inexpensively from industrial products or exhaust. [8, 14] Thus, considering the economic cost, direct CO conversion to high-value chemicals has attracted increasing attention in clean energy technology.[15, 16]

Copper-based material is the most widely studied electrocatalyst that facilities the reduction of CO to multi-carbon products.[17-19] However, the applicability in industry is still subject to their relatively high overpotential and low selectivity,[20, 21] leading to the need of exploring new and promising catalysts. Two-dimensional transition metal

carbide/nitride,[22, 23] known as MXene, has exhibited promising performance as electrocatalyst due to the large surface area, abundant active sites and excellent electrical conductivity.[24-28] MXene possesses a general formula of $M_{n+1}X_nT_x$ (n = 1-3), where M, X and T refer to the transition metal (M), carbon/nitrogen (C/N) and the terminated functional groups (T), such as -OH, -F or -O.[29] Pourbaix graph has indicated that a surface covered by -O is energetically favorable in most situation.[30] The -O group can be removed to create oxygen vacancy, resulting in exposed metal atom as active catalytic site.[31-34] On one hand, from early experimental study, it was reported that the exposed metal atoms on the Ti_3C_2 surface are able to capture CO_2 chemically, implying the potential application of MXene in CO_2/CO conversion.[35] On the other hand, a computational screening on MXene as CO_2RR electrocatalysts has shown the great potentiality of MXene family and the Mo_3C_2 was predicted to be a promising candidate as CO_2RR catalyst.[36] Recently, we also studied the defective hybrid MXene $Mo_2TiC_2O_2$, as a potential electrode for CO reduction toward CH_4.[37] By creating oxygen vacancy on the basal plane, a unique chemical environment was constructed which significantly promotes the CO reduction to hydrocarbon.

Inspired by aforementioned works, we took $Ti_3C_2O_2$, $Mo_3C_2O_2$ and $Mo_2TiC_2O_2$ as substrates, and designed catalysis systems with more spacious surface vacancy by removing two neighboring oxygen atoms to increase the local concentration of active sites and potentially enable the C-C coupling. Our DFT results demonstrated that the defective $Mo_2TiC_2O_2$ with a dual-oxygen vacancy (labeled as $Mo_2TiC_2O_2$-$2O_V$) exhibits superior activity and selectivity for CORR toward C_2 products. All the electrochemical reduction steps and the C-C bond coupling are feasible, with low limiting potential of -0.32 V *vs.* reversible hydrogen electrode (RHE).

2. Computational Details

The spin-polarized DFT calculations were performed by using the Vienna ab Initio Simulation Package (VASP).[38-40] The Perdew-Burke-Ernzerhof (PBE) functional[41] belonging to the generalized gradient in generalized gradient approximation (GGA)

was used to mimic the exchange-correlation effect, with the projector augmented wave (PAW) method[42] to describe ion-electron interaction. Cutoff energy for the plane-wave basis was set to be 450 eV. DFT-D3[43] correction was employed to consider van der Waals (vdW) interaction. The solvation effect was included by using the implicit solvation model in VASPsol, where the dielectric constant was set as 80.0 for water.[44] Three MXenes were studied as the substrates in this work: $Ti_3C_2O_2$, $Mo_3C_2O_2$ and $Mo_2TiC_2O_2$. Oxygen vacancy was created by removing two neighboring oxygen atoms on the surface. A vacuum layer of 15 Å in *z* direction was applied to avoid the interaction between periodic images. The effect of supercell size on the interaction to CO were evaluated according to adsorption energies of CO. The energy difference between the simulated adsorption energies in 4×4×1 and 3×3×1 supercell was less than 0.01 eV. Thus, we adopted 3×3×1 supercell in this work to save the computational cost. The Brillouin zone was sampled by a 3×3×1 Monkhorst-Pack k-point grid.[45] The convergence criteria of force and energy in our calculation were 0.02 eV $Å^{-1}$ and 10^{-4} eV respectively.

The Gibbs free energy change (ΔG) for each step of CORR process was calculated based on the computational hydrogen electrode (CHE) model proposed by Norskov et al:[46]

$$\Delta G = \Delta E + \Delta E_{ZPE} - T\Delta S$$

where ΔE, ΔE_{ZPE}, and ΔS are the change of total electronic energy in DFT, zero-point energy (ZPE) from the vibrational analysis and the entropy change between reactants and products, as shown in **Table S1**. The entropies of gas molecules were taken from the NIST database. The catalytic activity was evaluated through the limiting potential (U_L) *vs.* RHE that was defined as: [46]

$$U_L = -\Delta G_{max}/e$$

ΔG_{max} is the maximum free energy change of CORR process and *e* is the elementary charge. Transition state searches were conducted with the climbing-image nudged elastic band (CI-NEB) methods with four intermediate images for each step.[47]

In this work, we employed the widely used CHE model with implicit solvation treatment, which is routine and computation-saving. But we have to point out that this approach has certain limitations. The static calculation of intermediates and transition states crudely approximate crucially relevant entropic effects. The implicit solvation model that treats solvent as a structureless continuum cannot describe the interactions between key intermediates and electrolyte molecules, such as hydrogen bond that plays a critical role in the electrocatalytic reaction at the solid-liquid interface. Moreover, the influence of electric field is included too roughly. Recently, some new theoretical approaches have been established. For example, the constant potential method including few explicit water and continuum dielectric can reproduce a relatively reasonable electrochemical environment. [48, 49] Metadynamics simulation coupled with DFT-based molecular dynamics enables a more comprehensive sampling of the configurational space and hence describes free energy change in solvation more accurately.[50-52] We will try to apply these advanced methods in our following work.

3. Results and discussion

CO adsorption on the defective MXene surfaces

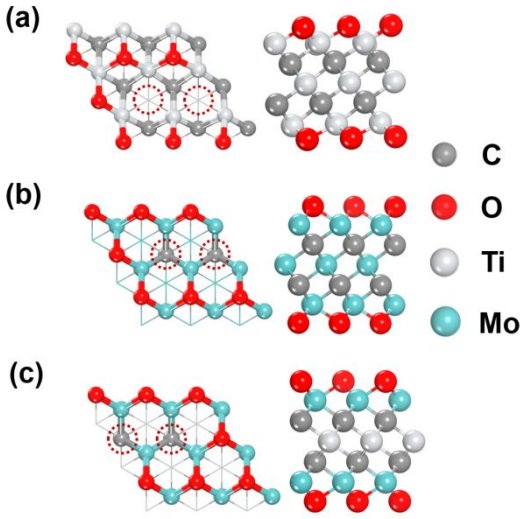

Figure 1. Top and side views of (a) $Ti_3C_2O_2$-$2O_V$, (b) $Mo_3C_2O_2$-$2O_V$ and (c) $Mo_2TiC_2O_2$-$2O_V$. The removed oxygen sites are marked in dashed circles.

There are two possible sites that the terminal oxygen occupies, namely the face-centered cubic (fcc) site and the hexagonal close-packed (hcp) site (**Figure S1**). First, we studied the most stable configurations of the terminal oxygen in the three materials. Theoretical optimization shows that the fcc site is energetically more favorable in $Ti_3C_2O_2$, whereas the oxygen at hcp site is more stable in $Mo_3C_2O_2$ and $Mo_2TiC_2O_2$, consistently with previous literature.[53] In experiment, there exist plenty of oxygen vacancies (O_V) on the exfoliated MXene surface,[34, 54] and the O_v can also be introduced by the incomplete terminal functionalization or partial reduction of the fully oxygen-covered plane.[34, 55-57] Our preceding work has shown that CO molecule can be captured by the exposed metal atoms at oxygen vacancy and then readily reduced to C_1 product, methane. Herein we propose that the C_2 products could be yielded if two neighboring oxygen atoms are removed to generate a more spacious vacancy. Formation energies of the first and second O_v are calculated to evaluate the feasibility of defective MXene following the reactions:

$$M_{n+1}X_nO_x + H_2 \rightarrow M_{n+1}X_nO\text{-}1O_v + H_2O \qquad E(1O_V);$$

$$M_{n+1}X_nO\text{-}1O_v + H_2 \rightarrow M_{n+1}X_nO\text{-}2O_v + H_2O \qquad E(2O_V).$$

Here the DFT energies of hydrogen and water molecules are used in the calculation. For the second leaving oxygen atom, both the sites close to and apart from the first vacancy are considered, corresponding to vacancy formation energies as $E(2O_V)_{dual}$ and $E(2O_V)_{separated}$, respectively. As listed in **Table 1**, $E(2O_V)$s are comparable to $E(1O_V)$, especially in the Mo-containing MXenes. Thus, if one oxygen is able to be removed, then a second oxygen atom can also be removed under similar conditions. Previous simulation also indicates that the surfaces covered by oxygen are stable. Even if the coverage of the surface groups is reduced by a quarter, the structural stability is largely unaffected.[58] We assume that the reductant capable of providing multiple electrons may remove two or more adjacent oxygen atoms simultaneously, such as $NaBH_4$ or $LiAlH_4$

that have been widely employed to treat oxygen-covered surfaces to generate defects.[59-61]

Table 1. The formation energies of various oxygen vacancies.

	$E(1O_V)$ / eV	$E(2O_V)_{dual}$ / eV	$E(2O_V)_{seperated}$ / eV
$Ti_3C_2O_2$	1.40	2.14	1.56
$Mo_3C_2O_2$	0.86	0.86	0.91
$Mo_2TiC_2O_2$	1.18	1.25	1.24

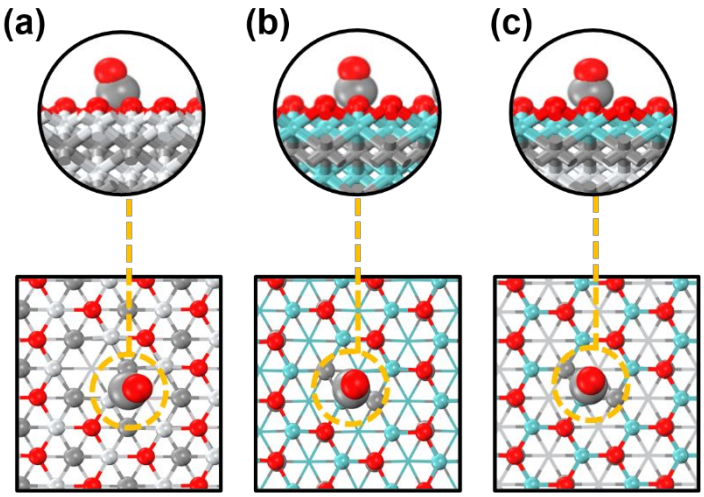

Figure 2. Adsorption configurations of one CO molecule on three surfaces (a) $Ti_3C_2O_2$-$2O_V$, (b) $Mo_3C_2O_2$-$2O_V$, and (c) $Mo_2TiC_2O_2$-$2O_V$. Color code: C, grey; O, red; Ti, light grey; Mo, cyan.

The adsorption of CO molecule in the vacancy is the first step of the whole CO reduction process. As shown in **Figure 2**. CO molecule tends to be trapped on the exposed metal atom within a carbon ending-on configuration. We mark adsorbed CO as $^*CO$ in which the asterisk represents the adsorption sites. The calculated binding free energies of the first $^*CO$ on $Ti_3C_2O_2$-$2O_v$, $Mo_3C_2O_2$-$2O_v$ and $Mo_2TiC_2O_2$-$2O_v$ are 0.48 eV, -0.54 eV and -0.89 eV respectively. The exothermic adsorption on $Mo_2TiC_2O_2$-$2O_V$

or $Mo_3C_2O_2$-$2O_V$ indicates that CO can be readily adsorbed on these two surfaces, while the $Ti_3C_2O_2$-$2O_V$ shows relatively weaker interaction with CO than other two defective MXenes. Thus, in later discussions, we will mainly focus on the $Mo_3C_2O_2$-$2O_v$ and $Mo_2TiC_2O_2$-$2O_v$. Since the dual-oxygen vacancy is created by removing two oxygen atoms, one more CO molecule is able to be captured to form (*CO)(*CO). Here the brackets denote the isolated adsorbed groups. For the adsorption of the second CO, the binding strengthens on $Mo_2TiC_2O_2$-$2O_V$ and $Mo_3C_2O_2$-$2O_V$ slightly decrease and the calculated binding free energies change to -0.39 eV and -0.41 eV respectively. Herein, the precursors to C_2 products are easily formed in $Mo_3C_2O_2$-$2O_v$ and $Mo_2TiC_2O_2$-$2O_v$ systems.

C-C coupling in the spacious vacancy

In electrocatalysis reduction process, proton-electron pairs attack the (*CO)(*CO) intermediate continuously. A thermochemical step of C-C bond formation is inserted between the electrochemical steps. C-C coupling that plays a critical role on the generation of C_2 products may take place between two *CO or other hydrogenated species, such as *CHO or *COH.[21] Considering the steric effect, hydrogen is unlikely to attack the buried carbon to form *CHO once two *CO groups are adsorbed.[37] Thus there are three possible steps of C-C bond formation that start from (*CO)(*CO), (*CO)(*COH) and (*COH)(*COH). The free energy changes of the electrochemical hydrogenation and coupling steps are listed in **Table 2**. One can see that the hydrogenation steps are spontaneous whereas the formation of new chemical bond is endothermic until (*COH)(*COH) is generated. Herein we suggest that the C-C coupling occurs between two *COH groups. In the vacancies of $Mo_3C_2O_2$-$2O_V$ and $Mo_2TiC_2O_2$-$2O_V$, the C-C distances in (*COH)(*COH) are 2.83 Å and 2.76 Å respectively. In comparison, the newly formed bond lengths are 1.42 Å and 1.40 Å, respectively, implying a stable double bond arises. The free energy changes illustrate that the dimerization of *COH on both $Mo_3C_2O_2$-$2O_V$ and $Mo_2TiC_2O_2$-$2O_V$ are

thermodynamically feasible. In addition, as shown in **Figure 3**, the CI-NEB-obtained activation energy barriers of *COH dimerization on $Mo_3C_2O_2$-$2O_V$ and $Mo_2TiC_2O_2$-$2O_V$ are 1.11 eV and 1.37 eV respectively. These simulated barriers are lower than that reported on Cu active surface (1.50 eV), which is able to be overcame at ambient condition.[62, 63] In comparison, on the metal surface, although the coupling between two hydrogenated carbonyl groups may be also feasible, the low concentration of *CHO or *COH on the surface limits the kinetics of dimerization and leads to a predominance of coupling in (*CO)(*CO) or (*CO)(*COH).[49, 64] In other words, the vacancy provides a unique environment that confines and enriches the active species, i.e., *COH, resulting in the higher activity of C-C coupling.

Table 2. Free energy changes of possible hydrogenation and C-C coupling steps after that two CO molecules have been adsorbed in the vacancy. ΔG_2^1 denotes to the free energy changes from intermediate 1 to intermediate 2.

	$\Delta G_{(*CO)(*COH)}^{(*CO)(*CO)}$ /eV	$\Delta G_{*CO*CO}^{(*CO)(*CO)}$ /eV	$\Delta G_{(*COH)(*COH)}^{(*CO)(*COH)}$ /eV	$\Delta G_{*CO*COH}^{(*CO)(*COH)}$ /eV	$\Delta G_{*COH*COH}^{(*COH)(*COH)}$ /eV
$Mo_2TiC_2O_2$-$2O_V$	-0.14	1.03	-0.07	0.60	0.08
$Mo_3C_2O_2$-$2O_V$	-0.06	0.78	-0.01	0.67	0.35

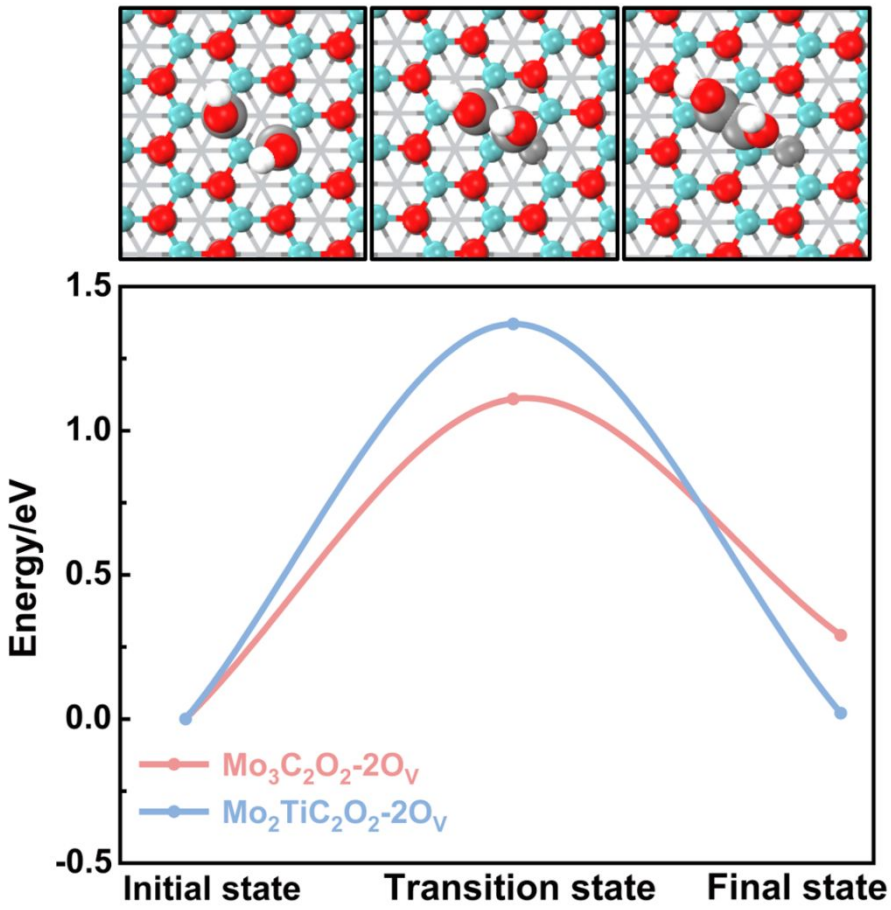

Figure 3. The reaction energy barriers of (*COH)(*COH) dimerization steps on $Mo_2TiC_2O_2$-$2O_v$ and $Mo_3C_2O_2$-$2O_v$.

Further reduction to C_2 products

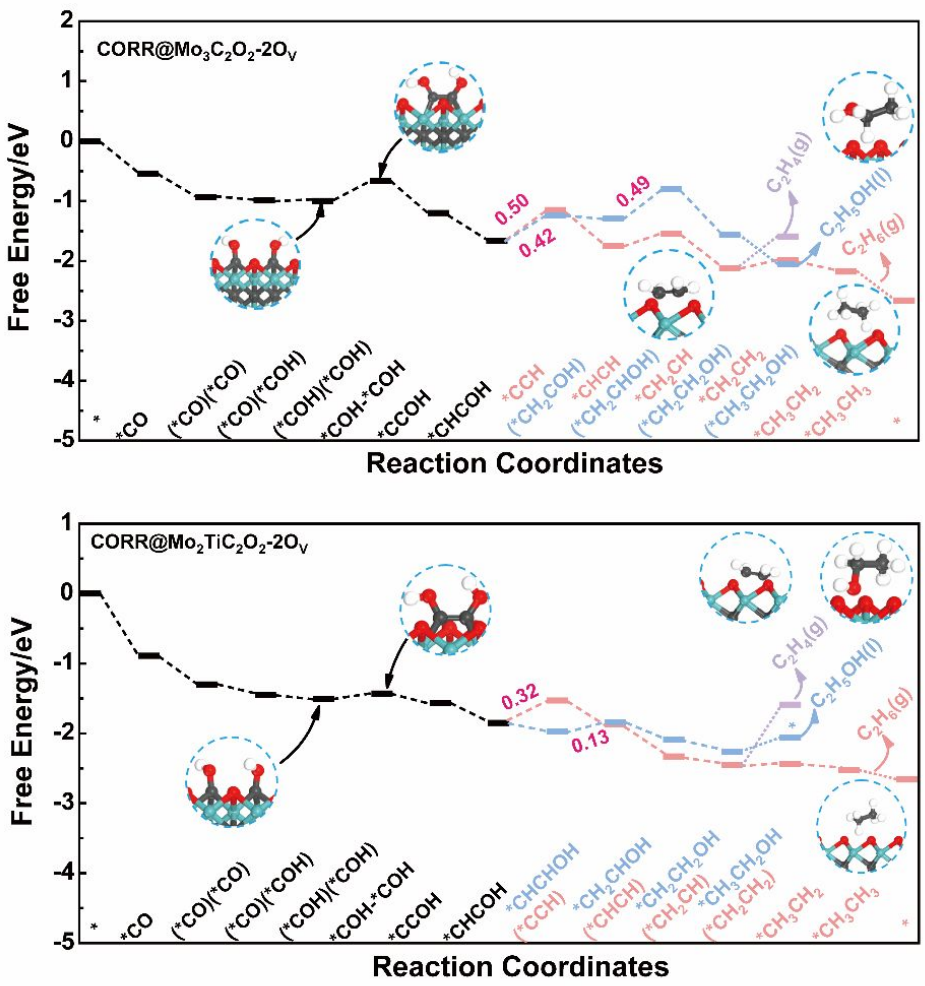

Figure 4. Free energy profiles of the whole CO reduction pathways on $Mo_3C_2O_2$-$2O_V$ and $Mo_2TiC_2O_2$-$2O_V$ at 0.0 V *vs.* RHE. The structures of key intermediates are depicted in the insets. Green, black, red and white balls represent Mo, C, O and H atoms, respectively.

The following steps to three common C_2 products, i.e., C_2H_4, C_2H_6 and C_2H_5OH, were investigated to determine the favorable pathways on $Mo_3C_2O_2$-$2O_v$ and $Mo_2TiC_2O_2$-$2O_v$. The whole free energy profiles are depicted in **Figure 4** and key information is summarized in **Table 3**. After C-C coupling between two *COH group, the protonation to *COH*COH proceeds to *CCOH with the removal of a water molecule. Then *CCOH is further reduced to *CHCOH, from which the pathways to hydrocarbons and ethanol are divided. If the next proton-electron pair reacts with the carbon in *CHCOH intermediate to generate *CHCHOH or $^*CH_2COH$, alcohol should be the main product. Otherwise, the protonation on the oxygen results in dehydration to *CCH and the subsequent route to hydrocarbons.

On $Mo_3C_2O_2$-$2O_v$, the step from *CHCOH to *CHCHOH is found to be energetically unfavorable with a barrier of 1.02 eV, while hydrogenation energetics to *CCH and $^*CH_2COH$ are comparable (0.50 eV vs. 0.42 eV). Herein the selectivity between hydrocarbons and ethanol may be relatively low. Among all the elementary steps, the formation of *CCH is the PDS with the maximum free energy change. The thermo-dynamical barriers of the subsequent hydrogenation steps to ethane or ethylene are all less than 0.20 eV, while the step from $^*CH_2CHOH$ to $^*CH_2CH_2OH$ on the path to ethanol exhibits a barrier of 0.49 eV. The energy barriers of PDS's to hydrocarbons and C_2H_5OH are comparable. There is only one relatively high barrier on the path to hydrocarbon, but two to C_2H_5OH. Besides, desorption of ethylene requires to overcome higher energy barrier than ethane. Herein ethane is suggested to be the major product.

In comparison, the deep reduction on $Mo_2TiC_2O_2$-$2O_V$ is thermodynamically feasible as well. Unlike $Mo_3C_2O_2$-$2O_v$ system, the Gibbs free energy barriers from *CHCOH to *CHCHOH is much lower than that to $^*CH_2COH$ on $Mo_2TiC_2O_2$-$2O_V$ (-0.19 eV vs. 0.90 eV). On the other hand, the hydrogenation of *CHCOH to *CCH requires energy change of +0.32 eV. We can roughly estimate the selectivity according to Arrhenius equation:

$$S = exp(|\Delta G_{key\text{-}intermediate}|/RT)$$

where $\Delta G_{key\text{-}intermediate}$ is the free energy difference between *CCH and *CHCHOH. Here the estimated selectivity is over 99%. Therefore, the path to ethanol is preferable in which the PDS is the generation of $^*CH_2CHOH$ with a barrier of 0.13 eV. The later

hydrogenation steps are all exothermic and desorption of ethanol is also energetically not hard to achieve. Therefore $Mo_2TiC_2O_2$-$2O_V$ is theoretically found to be an ideal electrocatalyst with both high activity and selectivity for CO reduction to ethanol.

Table 3. Summary of the whole reduction processes on various surfaces.

	PDS	ΔG_{PDS}/eV	Major Product
$Mo_3C_2O_2$-$2O_v$	*CHCOH→*CCH	0.50	C_2H_6
$Mo_2TiC_2O_2$-$2O_v$	*CHCOH→*CHCHOH	0.32	C_2H_5OH

Competition with C1 paths and HER

Although dual-oxygen vacancy is created, the CO reduction on an individual vacancy to C1 product is still possible and it could be a competing reaction of the C-C coupling. *CHO and *COH are two critical intermediates that lead to CH_4 or CH_3OH formation. As listed in **Table 4**, *CHO formation is more preferable than *COH, while the energy changes of both the two hydrogenation steps are positive, in contrast to the exothermic adsorption of the second CO. Besides, the addition of proton-electron pair becomes much easier after the adsorption of the second CO with a negative energy change. Since the vacancy has been occupied, (*CO)(*COH) tends to be generated rather than (*CO)(*CHO). Especially, for $Mo_2TiC_2O_2$-$2O_V$, both the hydrogenation energies to generate *CHO and *COH are higher than all the barriers on the pathway to ethanol. Therefore, $Mo_2TiC_2O_2$-$2O_V$ could possess high selectivity of ethanol over C_1 products.

Table 4. Gibbs free energy changes to different key intermediates

	ΔG^{*CO}_{*CHO}/eV	ΔG^{*CO}_{*COH}/eV	$\Delta G^{*CO}_{(*CO)(*CO)}$/eV	$\Delta G^{(*CO)(*CO)}_{(*CO)(*COH)}$/eV
$Mo_3C_2O_2$-$2O_V$	0.11	1.65	-0.39	-0.06
$Mo_2TiC_2O_2$-$2O_V$	0.33	0.72	-0.41	-0.14

Furthermore, the protons in solution can be captured by the active sites, resulting in the competitive hydrogen evolution reaction (HER) and low Faraday efficiency. The adsorption free energy of hydrogen (ΔG_{*H}) was calculated to evaluate the competition of HER. For $Mo_3C_2O_2$-$2O_V$ and $Mo_2TiC_2O_2$-$2O_V$, the ΔG_{*H}'s are 0.08 eV and -0.11 eV, respectively, indicating weaker adsorption than CO. Herein, the active sites are more likely to be occupied by CO and then CORR occurs. The binding of water to the active site was also considered, as shown in **Figure S2**. For $Mo_3C_2O_2$-$2O_V$ system, water with stronger binding (-0.59 eV vs. -0.54 eV) could hinder CO adsorption. While on $Mo_2TiC_2O_2$-$2O_V$, CO adsorption is more preferable than H_2O (-0.89 eV vs. -0.75 eV), suggesting that H_2O has little influence to the CORR on $Mo_2TiC_2O_2$-$2O_V$.

Insight into the unique property of Mo_2TiC_2-$2O_V$ system

To understand the enhancement of C-C coupling on $Mo_2TiC_2O_2$-$2O_V$, the electronic structure analysis was further performed. We focus on the *p*-orbitals of two carbon atoms in three intermediates, i.e., (*CO)(*CO), (*CO)(*COH) and (*COH)(*COH), in which two CO molecules have been trapped but C-C bond is not formed. As shown in the projected densities of states (pDOSs) plotted in **Figure 5(a)**, the *p*-orbitals of carbon atoms are mainly composed by the anti-bonding orbitals above the Fermi level. As the hydrogenation steps undergoing, electrons are filled into the anti-bonding orbitals of the carbonyl groups, leading to the down-shift of the *p*-bands of carbon atoms to valence band. In (*COH)(*COH), a large part of the *p*-band is below and close to the Fermi level, which is related to significantly activation of frontier orbitals. As a consequence, the C-C formation takes place between two adsorbed COH groups in (*COH)(*COH) intermediate.

On the other hand, according to the electronic effect on the C-C coupling, we believe that more electron transfer from catalyst to adsorbent can facilitate the formation of the multi-carbon products. To verify this point, the electron densities of $Mo_2TiC_2O_2$-$2O_V$ and $Mo_3C_2O_2$-$2O_V$ are compared in **Figure 5(b),** showing the electron density difference between these two homologous structures. Apparently, the defective

hybrid MXene, $Mo_2TiC_2O_2$-$2O_V$ exhibits higher electron density in the vacancy, suggesting that this substrate is able to donate more electrons to the adsorbed CO, subsequently strengthen the adsorption and eventually promote the dimerization of the carbonyl groups.

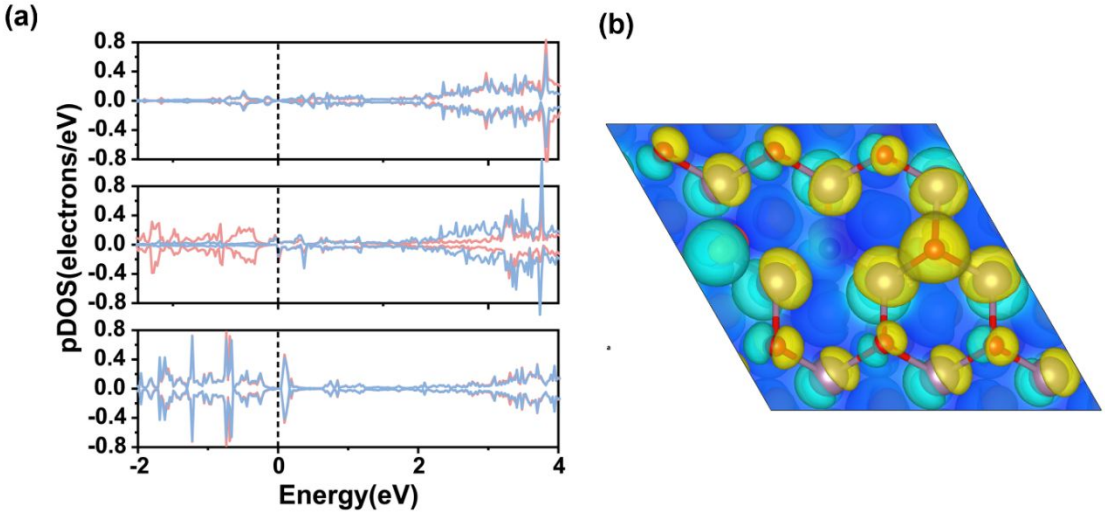

Figure 5. (a) The pDOS of *p*-bands of C atoms in carbonyl groups of (*CO)(*CO), (*CO)(*COH) and (*COH)(*COH). The red and blue lines are corresponding to the carbon atoms that are hydrogenated sequentially. (b) The charge density difference between $Mo_2TiC_2O_2$-$2O_V$ and $Mo_3C_2O_2$-$2O_V$. In yellow area, $Mo_2TiC_2O_2$-$2O_V$ system possesses higher electron density than $Mo_3C_2O_2$-$2O_V$, whereas in cyan area the electron density of $Mo_2TiC_2O_2$-$2O_V$ is lower.

4. Conclusion

In summary, by performing DFT calculations, we explored three MXene materials with dual surface vacancies as potential electrocatalysts for CORR to C_2 products. The vacancy was created by removing two neighboring oxygen atoms in the surface layer. DFT simulations demonstrate that $Mo_2TiC_2O_2$-$2O_V$ is a candidate for efficient electrocatalysis CORR to produce ethanol, with both the low overpotential and kinetic barriers as well as promising selectivity over C1 paths and HER. The energy change of

the PDS is only 0.32 eV, related to a less negative limiting potential of -0.32 V. The activation energy barrier of C-C coupling is calculated to be 1.37 eV, which is lower than that on copper surface. Moreover, the produced ethanol is easy to desorb from the active site. The electronic structure analysis shows that, as the carbonyl group is reduced to *COH species, the *p*-bands of C atoms shift down below Fermi level, which promotes the formation of the new C-C bond. The substrate with higher electron density in the vacancy, namely $Mo_2TiC_2O_2$-$2O_V$, can provide more electrons to carbon, herein possesses the best performance for electrocatalytic CORR. Our work shows the potentiality of defective $Mo_2TiC_2O_2$ as the electrocatalyst for CORR and provide a possible strategy to improve the performance of MXene electrocatalysts by creating spacious oxygen vacancy. We hope to have the opportunity to collaborate with experiments in the future to realize our theoretical hypothesis.

Conflicts of interest

There are no conflicts to declare

Acknowledgement

This work was supported by the National Science Foundation of China (No. 21803074), the “From 0 to 1” Innovative program of CAS (No. ZDBS-LY-JSC021), Ningbo S&T Innovation 2025 Major Special Program (No: 2018B10016), Natural Science Foundation of Zhejiang Province (No. D21E020002), K. C. Wong Education Foundation (GJTD-2019-13) and Fujian Institute of Innovation, Chinese Academy of Sciences. This research used computational resources of the High-Performance Computing Center of Collaborative Innovation Center of Advanced Microstructures, Nanjing University. Part of this work (C.Z.) was performed under the auspices of the U.S. Department of Energy by Lawrence Livermore National Laboratory under

Contract DE-AC52-07NA27344. C.Z. is partially supported by the PLS-Postdoctoral Grant of the Lawrence Livermore National Laboratory.

Reference

1. W. Wang, S. Wang, X. Ma and J. Gong, *Chem. Soc. Rev.*, 2011, **40**, 3703-3727.
2. M. Asadi, K. Kim, C. Liu, A. V. Addepalli, P. Abbasi, P. Yasaei, P. Phillips, A. Behranginia, J. M. Cerrato, R. Haasch, P. Zapol, B. Kumar, R. F. Klie, J. Abiade, L. A. Curtiss and A. Salehi-Khojin, *Science*, 2016, **353**, 467-470.
3. W. Zhang, Y. Hu, L. Ma, G. Zhu, Y. Wang, X. Xue, R. Chen, S. Yang and Z. Jin, *Adv Sci (Weinh)*, 2018, **5**, 1700275.
4. D. T. Whipple and P. J. A. Kenis, *J. Phys. Chem. Lett.*, 2010, **1**, 3451-3458.
5. Z. Q. Tian, C. Priest and L. Chen, *Adv. Theory Simul.*, 2018, **1**, 23.
6. M. Jouny, W. Luc and F. Jiao, *Ind. Eng. Chem. Res.*, 2018, **57**, 2165-2177.
7. C. Xia, P. Zhu, Q. Jiang, Y. Pan, W. T. Liang, E. Stavitsk, H. N. Alshareef and H. T. Wang, *Nat. Energy*, 2019, **4**, 776-785.
8. Y. Y. Birdja, E. Perez-Gallent, M. C. Figueiredo, A. J. Gottle, F. Calle-Vallejo and M. T. M. Koper, *Nat. Energy*, 2019, **4**, 732-745.
9. H. Mistry, A. S. Varela, C. S. Bonifacio, I. Zegkinoglou, I. Sinev, Y. W. Choi, K. Kisslinger, E. A. Stach, J. C. Yang, P. Strasser and B. Roldan Cuenya, *Nat. Commun.*, 2016, **7**, 8.
10. C. T. Dinh, T. Burdyny, M. G. Kibria, A. Seifitokaldani, C. M. Gabardo, F. P. G. de Arquer, A. Kiani, J. P. Edwards, P. De Luna, O. S. Bushuyev, C. Q. Zou, R. Quintero-Bermudez, Y. J. Pang, D. Sinton and E. H. Sargent, *Science*, 2018, **360**, 783-787.
11. J. Gao, H. Zhang, X. Y. Guo, J. S. Luo, S. M. Zakeeruddin, D. Ren and M. Gratzel, *J. Am. Chem. Soc.*, 2019, **141**, 18704-18714.
12. D. Higgins, A. T. Landersp, Y. F. Ji, S. Nitopi, C. G. Morales-Guio, L. Wang, K. R. Chan, C. Hahn and T. F. Jaramillo, *ACS Energy Lett.*, 2018, **3**, 2947-2955.
13. D. Karapinar, N. T. Huan, N. R. Sahraie, J. K. Li, D. Wakerley, N. Touati, S. Zanna, D. Taverna, L. H. G. Tizei, A. Zitolo, F. Jaouen, V. Mougel and M. Fontecave, *Angew. Chem.-Int. Edit.*, 2019, **58**, 15098-15103.
14. M. Jouny, W. Luc and F. Jiao, *Nat. Catal.*, 2018, **1**, 1002-1002.
15. C. W. Lee, N. H. Cho, S. W. Im, M. S. Jee, Y. J. Hwang, B. K. Min and K. T. Nam, *J. Mater. Chem. A*, 2018, **6**, 14043-14057.
16. C. W. Li, J. Ciston and M. W. Kanan, *Nature*, 2014, **508**, 504-+.
17. H. Xiao, T. Cheng, W. A. Goddard and R. Sundararaman, *J. Am. Chem. Soc.*, 2016, **138**, 483-486.
18. H. Xie, T. Y. Wang, J. S. Liang, Q. Li and S. H. Sun, *Nano Today*, 2018, **21**, 41-54.
19. J. Zhao, S. Xue, J. Barber, Y. W. Zhou, J. Meng and X. B. Ke, *J. Mater. Chem. A*, 2020, **8**, 4700-4734.

20. M. B. Gawande, A. Goswami, F. X. Felpin, T. Asefa, X. X. Huang, R. Silva, X. X. Zou, R. Zboril and R. S. Varma, *Chem. Rev.*, 2016, **116**, 3722-3811.
21. S. Nitopi, E. Bertheussen, S. B. Scott, X. Y. Liu, A. K. Engstfeld, S. Horch, B. Seger, I. E. L. Stephens, K. Chan, C. Hahn, J. K. Norskov, T. F. Jaramillo and I. Chorkendorff, *Chem. Rev.*, 2019, **119**, 7610-7672.
22. B. Anasori, M. R. Lukatskaya and Y. Gogotsi, *Nature Reviews Materials*, 2017, **2**, 17.
23. B. Anasori, Y. Xie, M. Beidaghi, J. Lu, B. C. Hosler, L. Hultman, P. R. C. Kent, Y. Gogotsi and M. W. Barsoum, *ACS Nano*, 2015, **9**, 9507-9516.
24. Z. H. Fu, N. Wang, D. Legut, C. Si, Q. F. Zhang, S. Y. Du, T. C. Germann, J. S. Francisco and R. F. Zhang, *Chem. Rev.*, 2019, **119**, 11980-12031.
25. L. Li, X. Y. Wang, H. R. Guo, G. Yao, H. B. Yu, Z. Q. Tian, B. H. Li and L. Chen, *Small Methods*, 2019, **3**, 7.
26. D. S. Wang, F. Li, R. Q. Lian, J. Xu, D. X. Kan, Y. H. Liu, G. Chen, Y. Gogotsi and Y. J. Wei, *ACS Nano*, 2019, **13**, 11078-11086.
27. B. Huang, N. G. Zhou, X. Z. Chen, W. J. Ong and N. Li, *Chem.-Eur. J.*, 2018, **24**, 18479-18486.
28. Y. Guo, T. R. Wang, Q. Yang, X. L. Li, H. F. Li, Y. K. Wang, T. P. Jiao, Z. D. Huang, B. B. Dong, W. J. Zhang, J. Fan and C. Y. Zhi, *ACS Nano*, 2020, **14**, 9089-9097.
29. M. R. Lukatskaya, O. Mashtalir, C. E. Ren, Y. Dall'Agnese, P. Rozier, P. L. Taberna, M. Naguib, P. Simon, M. W. Barsoum and Y. Gogotsi, *Science*, 2013, **341**, 1502-1505.
30. Z. W. Seh, K. D. Fredrickson, B. Anasori, J. Kibsgaard, A. L. Strickler, M. R. Lukatskaya, Y. Gogotsi, T. F. Jaramillo and A. Vojvodic, *ACS Energy Lett.*, 2016, **1**, 589-594.
31. F. Bai, L. Xu, X. Y. Zhai, X. Chen and W. S. Yang, *Adv. Energy Mater.*, 2020, **10**, 19.
32. D. Zhao, Z. Chen, W. J. Yang, S. J. Liu, X. Zhang, Y. Yu, W. C. Cheong, L. R. Zheng, F. Q. Ren, G. B. Ying, X. Cao, D. S. Wang, Q. Peng, G. X. Wang and C. Chen, *J. Am. Chem. Soc.*, 2019, **141**, 4086-4093.
33. J. H. Peng, X. Z. Chen, W. J. Ong, X. J. Zhao and N. Li, *Chem*, 2019, **5**, 18-50.
34. J. Q. Zhang, Y. F. Zhao, X. Guo, C. Chen, C. L. Dong, R. S. Liu, C. P. Han, Y. D. Li, Y. Gogotsi and G. X. Wang, *Nat. Catal.*, 2018, **1**, 985-992.
35. I. Persson, J. Halim, H. Lind, T. W. Hansen, J. B. Wagner, L. A. Naslund, V. Darakchieva, J. Palisaitis, J. Rosen and O. A. Persson, *Adv. Mater.*, 2019, **31**, 5.
36. N. Li, X. Z. Chen, W. J. Ong, D. R. MacFarlane, X. J. Zhao, A. K. Cheetham and C. H. Sun, *ACS Nano*, 2017, **11**, 10825-10833.
37. L. Li, B. H. Li, H. R. Guo, Y. L. Li, C. H. Sun, Z. Q. Tian and L. Chen, *Nanoscale*, 2020, **12**, 15880-15887.
38. G. Kresse and J. Furthmuller, *Comput. Mater. Sci.*, 1996, **6**, 15-50.
39. G. Kresse and J. Hafner, *Phys. Rev. B*, 1996, **54**, 11169.
40. G. Kresse and J. Hafner, *Phys Rev B Condens Matter*, 1994, **49**, 14251-14269.
41. J. P. Perdew, K. Burke and M. Ernzerhof, *Phys. Rev. Lett.*, 1996, **77**, 3865-3868.
42. G. Kresse, *Phys. Rev. B*, 1999, **59**, 1758.
43. S. Grimme, J. Antony, S. Ehrlich and H. Krieg, *J. Chem. Phys.*, 2010, **132**, 19.

44. K. Mathew, R. Sundararaman, K. Letchworth-Weaver, T. A. Arias and R. G. Hennig, *J. Chem. Phys.*, 2014, **140**, 8.
45. H. J. Monkhorst and J. D. Pack, *Physical Review B*, 1976, **13**, 5188-5192.
46. J. K. Norskov, J. Rossmeisl, A. Logadottir, L. Lindqvist, J. R. Kitchin, T. Bligaard and H. Jonsson, *J. Phys. Chem. B*, 2004, **108**, 17886-17892.
47. G. Henkelman, B. P. Uberuaga and H. Jonsson, *J. Chem. Phys.*, 2000, **113**, 9901-9904.
48. H. Xiao, T. Cheng and W. A. Goddard, *J. Am. Chem. Soc.*, 2017, **139**, 130-136.
49. J. D. Goodpaster, A. T. Bell and M. Head-Gordon, *J. Phys. Chem. Lett.*, 2016, **7**, 1471-1477.
50. G. Cassone, F. Pietrucci, F. Saija, F. Guyot and A. M. Saitta, *Chem. Sci.*, 2017, **8**, 2329-2336.
51. M. Ferus, F. Pietrucci, A. M. Saitta, O. Ivanek, A. Knizek, P. Kubelik, M. Krus, L. Juha, R. Dudzak, J. Dostal, A. Pastorek, L. Petera, J. Hrncirova, H. Saeidfirozeh, V. Shestivska, J. Sponer, J. E. Sponer, P. Rimmer, S. Civis and G. Cassone, *Astron. Astrophys.*, 2019, **626**, 21.
52. F. Pietrucci and A. M. Saitta, *Proc. Natl. Acad. Sci. U. S. A.*, 2015, **112**, 15030-15035.
53. L. H. Li, *Comput. Mater. Sci.*, 2016, **124**, 8-14.
54. X. H. Sang, Y. Xie, M. W. Lin, M. Alhabeb, K. L. Van Aken, Y. Gogotsi, P. R. C. Kent, K. Xiao and R. R. Unocic, *ACS Nano*, 2016, **10**, 9193-9200.
55. W. Zhou, X. L. Zou, S. Najmaei, Z. Liu, Y. M. Shi, J. Kong, J. Lou, P. M. Ajayan, B. I. Yakobson and J. C. Idrobo, *Nano Lett.*, 2013, **13**, 2615-2622.
56. C. Y. Shi, M. Beidaghi, M. Naguib, O. Mashtalir, Y. Gogotsi and S. J. L. Billinge, *Phys. Rev. Lett.*, 2014, **112**, 5.
57. L. H. Karlsson, J. Birch, J. Halim, M. W. Barsoum and P. O. A. Persson, *Nano Lett.*, 2015, **15**, 4955-4960.
58. M. Ashton, K. Mathew, R. G. Hennig and S. B. Sinnoet, *J. Phys. Chem. C*, 2016, **120**, 3550-3556.
59. H. Q. Tan, Z. Zhao, W. B. Zhu, E. N. Coker, B. S. Li, M. Zheng, W. X. Yu, H. Y. Fan and Z. C. Sun, *ACS Appl. Mater. Interfaces*, 2014, **6**, 19184-19190.
60. M. Asnavandi, Y. C. Yin, Y. B. Li, C. H. Sun and C. Zhao, *ACS Energy Lett.*, 2018, **3**, 1515-1520.
61. K. Raagulan, R. Braveenth, B. M. Kim, K. J. Lim, S. B. Lee, M. Kim and K. Y. Chai, *RSC Adv.*, 2020, **10**, 1613-1633.
62. J. H. Montoya, A. A. Peterson and J. K. Nørskov, *ChemCatChem*, 2013, **5**, 737-742.
63. T. W. He, K. Reuter and A. J. Du, *J. Mater. Chem. A*, 2020, **8**, 599-606.
64. K. Jiang, R. B. Sandberg, A. J. Akey, X. Y. Liu, D. C. Bell, J. K. Norskov, K. R. Chan and H. T. Wang, *Nat. Catal.*, 2018, **1**, 111-119.